Sensitivity Study of Turbulent Flow Simulations Over a Rotating Disk

Michael A. Snider[1] and Svetlana V. Poroseva[2]
University of New Mexico, Albuquerque, New Mexico, 87131

With increasing demand for renewable energy, there is a need for accurate and reliable simulations of a flow around a wind turbine. To be of use as an engineering design and planning tool, such simulations should be conducted in a timely manner. This can be achieved if a flow is modeled with Reynolds-Averaged Navier-Stokes turbulence models. To reduce uncertainties associated with numerical simulations from the simulation results, one has to ensure the convergence of results with respect to various simulation parameters. In this paper, the effect of the size of computational domain, boundary proximity, grid stretching, and initial grid wall spacing is analyzed. Simulations are conducted with several turbulence models using structured meshes. Due to the complex geometry of wind turbines, a flow over an infinite rotating disk is considered in the current paper as a first step. Such flow represents a rotating wind turbine with an infinite number of blades.

Nomenclature

C_f = *skin friction coefficient,* $\tau_w / \left(\rho U_\infty^2 / 2\right)$
q^2 = *twice the turbulent kinetic energy,* $q^2 = \overline{u'^2} + \overline{v'^2} + \overline{w'^2}$
r = *radial position on infinite disk measured from axis of rotation*
Re = *Reynolds number,* $\omega r^2/\nu$
$Re_{\delta 2}$ = *momentum thickness Reynolds number,* $\omega r\delta_2/\nu$
u_r = *laminar flow radial velocity component*
u_z = *laminar flow axial velocity component*
u_θ = *laminar flow tangential velocity component*
u = *instantaneous tangential velocity in rotating reference frame*
u' = *tangential velocity fluctuation in rotating reference frame*
v = *instantaneous axial velocity*
v' = *axial velocity fluctuation*
w = *instantaneous radial velocity*
w' = *radial velocity fluctuation*
y = *physical distance normal to rotating disk's surface (axial direction)*
y^+ = *non-dimensional distance normal to rotating disk's surface,* $y\mu_\tau/\nu$
U = *mean tangential velocity in rotating reference frame*
U^+ = *mean velocity in tangential direction in wall units,* U/μ_τ
U_∞ = *Local disk surface speed,* ωr
$|U|$ = *mean velocity vector magnitude*
W = *mean radial velocity*
δ_2 = *momentum thickness,* $\delta_2 = \int_0^\infty \frac{U}{U_\infty}\left(1 - \frac{U}{U_\infty}\right) dy$
ρ = *fluid density*
μ_τ = *friction velocity in tangential direction,* $U_\infty\sqrt{C_f/2}$
τ = *shear stress vector magnitude*

[1]Graduate Student, Mechanical Engineering, MSC01 1105, 1 UNM Albuquerque, NM 87131-0001, AIAA Student.
[2]Assistant professor, Mechanical Engineering, MSC01 1105, 1 UNM Albuquerque, NM 87131-0001, AIAA Senior Member.

ω = *angular velocity (rad/s)*
ν = *kinematic viscosity*
τ_w = *wall shear stress,* $\rho\sqrt{\overline{u'v'}^2 + \overline{v'w'}^2}$
SR = *axial stretch ratio of grid cells*

I. Introduction

WITH the increased demand for clean energy and reduced carbon emission, there has been substantial growth in the wind energy industry in the past decade. This trend is expected to continue. IBIS World reports that the wind energy industry is expected to experience the second highest rate of the revenue growth from 2010 to 2016 compared to other national industry sectors.[1] Wind energy production is estimated to generate 1.92% of the world's electricity by the end of 2011 and 9.1% of the electricity demand by 2020[2].

To achieve these goals, it is important to better understand and predict the behavior of a flow around a wind turbine as this is a key for designing efficient wind turbines and planning wind farms. A valuable insight into the flow dynamics and fluid–structure interaction can be obtained through numerical simulations. However, the scale of the problem and the flow complexity limit the choice of computational tools available for conducting accurate simulations. Indeed, requirements for the computational grid resolution and the range of Reynolds numbers of interest make both Direct Numerical Simulations and Large Eddy Simulations computationally unfeasible. Flow simulations with the Reynolds-Averaged Navier-Stokes (RANS) turbulence models, on the other hand, seem to be a reasonable choice. They can be conducted in a wide range of Reynolds numbers without any limitation, simulations are computationally inexpensive, and numerical codes are easily accessible as commercial or publicly available software. Therefore, this approach is adopted in our study.

A problem with any numerical simulations including RANS simulations is how to ensure that their results correctly reproduce features of interest of a real flow. This is of particular importance for a flow around a wind turbine as experimental and observational data are scarce. A necessary step is to conduct a sensitivity analysis of simulation results with respect to the choice of a turbulence model and model parameters, the size of a computational domain, grid resolution, boundary and initial conditions, and the accuracy of implemented numerical schemes among other factors.

In industry, a typical practice is to rely on commercial software for conducting simulations. It means that only a limited number of simulation parameters can vary. The current study seeks to analyze the convergence of simulation results with respect to the size of computational domain, boundary proximity, grid stretching, and initial grid wall spacing. These parameters were chosen following the recommendations for CFD calculations in the NASA's OVERFLOW 2.1 user manual[3]. They are also available to vary in Star-CCM+ software[4], a CFD package commonly used in industry and utilized in the current study. A turbulent flow was modeled with a few standard RANS models: a one-equation Spalart-Allmaras model[5], two-equation k - ε and k – ω models[6,7], SST[8] and RST[9] models.

Due to the geometric complexity of wind turbines, as a first step, simulations of a flow over a rotating disk have been conducted. Indeed, with the number of blades on a wind turbine approaching infinity, the turbine's geometry transforms to a solid disk. Also assumed is that the disk has an infinite radius. This flow is an excellent test case, because the analytical solution for laminar flows and extensive experimental and LES databases for turbulent flows are available.

The first person that derived a solution for the laminar flow field of a stationary fluid subjected to an infinite disk's rotation was Theodore von Karman[10]. He reformulated the Navier-Stokes equations in terms of a non-dimensional height and derived an approximate solution from the integral form of the boundary layer equation. Cochran[11] improved upon the von Karman's work and numerically obtained an accurate representation of the exact solution in this flow. White[12], expanding on the Cochran's solution, lengthened the solution's domain infinitely above the disk's surface.

Wu and Squires[13] conducted LES simulations of a flow over a rotating disk and compared their results with the experimental data of Little and Eaton[14].

In Little and Eaton[14], the experimental set was a rotating disk of one-meter diameter in an otherwise static air volume. The only motion of the fluid was due to the disk's rotation. Measurements were taken at a variety of angular velocities and radial positions in the flow field. Kobayashi, Kohama and Takamadate[15] experimentally studied the boundary layer transition in this flow geometry from laminar to turbulent. The experiment was conducted to find the Reynolds number at which the onset of instability and the onset of turbulence occurred in the boundary layer. Particular attention in their work was given to formation of spiral vortices in the transition regime.

In our study, laminar and turbulent flows over an infinite rotating disk are simulated. Laminar flow solutions are compared with the Cochran's solution. Turbulent flow simulations are compared with the data of Little and Eaton[14]. Sensitivity analysis is conducted for both laminar and turbulent flows. This work will be used as a stepping stone to the creation of computational domains that will be suitable for accurate and reliable wind turbine simulations.

II. Simulation Parameters

A. Computational Domain

An initial domain size of 1x5x5 meters in axial, radial and tangential directions, respectively, was chosen as the control volume to simulate a flow over a rotating infinite disk. The domain is shown in Fig. 1 along with the location of the line probe at r = 0.421 meters where the experimental data were sampled.

This is the smallest size of a computational domain for all laminar flow simulations. Larger sizes did not result in any improvement of the accuracy of simulation results in a laminar flow.

Initial turbulent flow simulations were computed on this domain size. The computational domain size was varied in all three dimensions in this sensitivity study. Specifically, the radial and tangential dimensions were shortened while the axial dimension remained constant. Then, the axial dimension was reduced, while the radial and tangential dimensions were held constant.

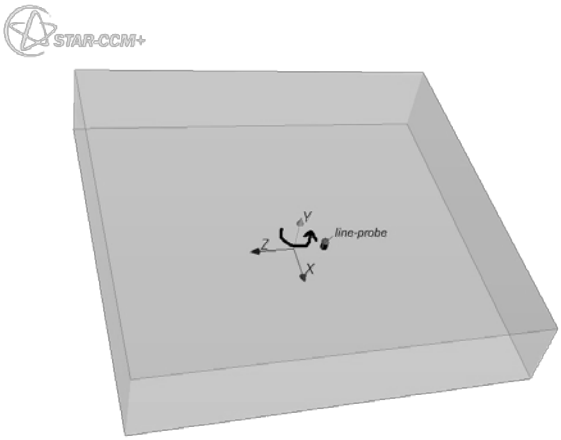

Figure 1. 1x5x5 meter Computational domain. *Computational domain with line probe, located at r=0.421 meters, highlighted. And rotation direction (+Y-axis) displayed.*

The computational domain and grids were generated in ICEM[16] and then imported into Star-CCM+[4].

B. Grid

The structured grid resolution in the initial computational domain was set to be 16x50x50 nodes in the axial, radial, and tangential directions, respectively, for laminar flow simulations at Re = 1000 at a radius of 1 m. For turbulent flow simulation at $Re = 10^6$ at a radius of 0.421 m, the grid refinement was varied drastically throughout this study. The grid resolution changed for each simulation as a function of the computational domain size, initial grid wall spacing, and grid stretching.

Initial grid wall spacing is a distance from the disk surface in the axial direction at which the first cell's centroid is placed. It is determined in standard non-dimensional y^+ units.

Simulations were conducted with the initial grid wall spacing y^+ = 5, 10, 20, 30, 40, 50, 75, 100 and 200.

Grid stretching is defined as the ratio of a cell's axial length to the axial length of the adjacent cell closer to the disk's surface. Simulations were conducted with a grid stretching ratio of 1.1, 1.2, 1.3, 1.5 and 2.0.

C. Boundary Conditions

The disk's surface is represented by a wall with a no-slip condition with an assigned value of the angular velocity about the rotation axis, +Y-axis as seen in Fig.1. A velocity inlet is chosen as a boundary condition for a flow entering the computational domain. The remaining side boundaries are pressure outlets with a prescribed gage pressure of zero. This allows fluid to leave the computational domain through these boundaries without returning back into the domain. The fluid velocity at the inlet is set as an input parameter in Star-CCM+[4].

III. Numerical Method

Star-CCM+[4] uses a first and second-order upwind calculation for its convection term. The choice of using one model over another can significantly affect the stability and accuracy of the numerical scheme. For this work, the second-order upwind scheme is used. Although more accurate, it is more computationally demanding and in some simulations the solution convergence properties can be poor due to reduced numerical dissipation.

IV. Turbulence Models

The five turbulence models that will be used in this study are:

- Standard k - ε [6]
- Standard $k - \omega$ [7]
- SST[8]
- High-Reynolds Number Spalart-Allmaras[5]
- Reynolds Stress Transport (RST)[9]

A. Standard k - ε Model

The k - ε turbulence model is a two-equation model in which transport equations are solved for the turbulent kinetic energy and its dissipation rate. Many forms of the k - ε model have been in use for several decades, and it has become the most widely used model for industrial applications.

This type of turbulence models requires additional flow modeling near walls. In the current study the High y^+ Wall Treatment was chosen from the options available in Star-CCM+[4] as the wall function for this model (more discussion on the wall treatment options available in Star-CCM+[4] is provided in Section IV.F). This option is equivalent to the traditional wall function approach, where the relation $U^+ = y^+$ is enforced in the near wall region. In Star-CCM+[4] the High y^+ Wall Treatment is classified as a standard wall law, which is slope-discontinuous between the laminar and turbulent profiles.

In this work, the standard values of the model coefficients are used, as shown in Table 1.

Table 1. Standard k - ε Coefficients Used in Star-CCM+

$C_{\varepsilon 1}$	$C_{\varepsilon 2}$	C_μ	C_M	σ_ε	σ_k
1.44	1.92	0.09	2.0	1.3	1.0

B. Standard k - ω Model

The k - ω model is also a two-equation model in which the transport equations are solved for the turbulent kinetic energy and the specific dissipation rate, that is, the dissipation rate per unit turbulent kinetic energy. This model is also paired with the High y^+ Wall Treatment mentioned in the previous model. The k - ω model is used with the standard values of the model coefficients:

Table 2. Standard k - ω Coefficients Used in Star-CCM+

α	β	β^*	σ_k	σ_ω
0.52	0.072	0.09	0.5	0.5

C. SST Model

The SST (shear-stress transport) model is a two-equation model that blends together the transport equations of the standard k - ε model and the k - ω model. This model is also combined with the High y^+ Wall Treatment model. The model coefficients used in the SST model simulations are shown in Table 3.

Table 3. Standard SST Coefficients Used in Star-CCM+

a_1	β_1	β_2	β^*	κ	σ_{k1}	σ_{k2}	$\sigma_{\omega 1}$	$\sigma_{\omega 2}$
0.31	0.075	0.0828	0.09	0.41	0.85	1.0	0.5	0.856

D. High-Reynolds Number Spalart-Allmaras Model

The High-Reynolds Number Spalart-Allmaras turbulence model solves a single transport equation for the turbulent viscosity. This model is a modification of the standard Spalart-Allmaras[5] turbulence model developed by the authors of Star-CCM+[4]. In the model, the viscous damping within the buffer layer and viscous sublayer is not included. This model utilizes the High y^+ Wall Treatment model.

In this work, the model is used with the coefficients given in Table 4.

Table 4. High-Reynolds Number Spalart-Allmaras Coefficients Used in Star-CCM+

C_{b1}	C_{b2}	C_{prod}	C_{w2}	C_{w3}	κ	σ
0.1335	0.622	2.0	0.3	2.0	0.41	0.667

E. Reynolds Stress Transport Model

Star-CCM+[4] has a choice of three different Reynolds stress transport turbulence models. In the current study, the Linear Pressure Strain model[9] has been used. The RST model also utilizes the High y^+ Wall Treatment model. The turbulent dissipation rate is modeled as in the k - ε turbulence model, but with different coefficients as seen in Table 5. The turbulent diffusion term is used in isotropic form[17].

Table 5. RSTM Linear Pressure Strain Dissipation Rate Coefficients Used in Star-CCM+

$C_{\varepsilon 1}$	$C_{\varepsilon 2}$
1.44	1.92

F. Wall Modeling

Star-CCM+[4] provides three options to resolve the near-wall flow physics:

- High y^+ Wall Treatment
- Low y^+ Wall Treatment
- All y^+ Wall Treatment

In order to obtain a level of consistency between simulations conducted with different models, choosing a wall function that is available for all five turbulence models is essential. From the three options, only the High y^+ Wall Treatment is available in Star-CCM+[4] for all turbulence models. Therefore, it was used in all simulations in this study.

The High y^+ Wall function model requires that the initial cell's centroid lies within the logarithmic region of flow. Inaccuracies arise when this approach is used in combination with a grid that is too refined near the wall. This wall function segregates the viscous dominated laminar region from the turbulence region and applies the wall law $U^+ = y^+$ in the laminar region and the log law in the turbulent region. Star-CCM+[4] recommends that the wall cell's centroid location be greater than $y^+ = 30$, warning that significant error can occur if the centroid is placed closer than $y^+ = 12$. This wall function is only recommended for high Reynolds number simulations. Hence the "High" in this wall function's title.

Star-CCM+[4] warns of the inaccuracy danger of using any model other than the All-y^+ model, but due to the simple geometry of a rotating infinite disk where the Reynolds number is known along the radius, we found the High y^+ Wall Treatment to be acceptable.

V. Results

The case of a laminar flow over an infinite rotating disk was studied at a Reynolds number of 1000. The results obtained were compared with the Cochran's solution[11] to validate Star-CCM+[4] solutions and to determine the size of the computational domain for the initial turbulent flow simulations. Turbulent flow simulations were conducted at $Re = 10^6$.

Computations have been conducted using high-performance computing systems available through the Center for Advanced Research Computing at the University of New Mexico. Specifically, the 36-node Nano Linux cluster (2 Intel Xeon 5140 (2.33 GHz) processors per node, 2 cores per processor, 8GB RAM/node, 1300 GFlops) has been used for simulations that were run on up to 8 nodes of the system. A desktop computer was also used for less computationally demanding simulations (Windows 7, 64-bit, Intel Core i7-2600, 3.40GHz, 8GB RAM).

A. Laminar Flow

The size of the computational domain was varied in a laminar flow simulation, but the grid cell size was kept the same. That is, as the computational domain became smaller, the number of cells within the domain decreased. The grids in these laminar simulations had an initial grid wall spacing of y^+=1 (0.01 meters) and a grid stretching of 1.2 in the axial direction. In the radial and tangential direction, there was a uniform cell length of 0.1 meters. The physical dimension above the disk in which the data were sampled was extended to approximately 0.3 meters.

Results of the laminar flow simulations for two different sizes of the computational domain are shown in Figs. 2 and 3. Close agreement is demonstrated between the simulation results and the Cochran's solution in both cases.

The data was sampled at a radius of 1 *m* on an infinite disk for the Reynolds number of 1000. The data has been smoothed by linearly interpolating the node values.

The laminar flow solution showed no sensitivity in respect to the size of the computational domain. Therefore, the smallest domain was chosen for conducting the initial turbulent flow simulations.

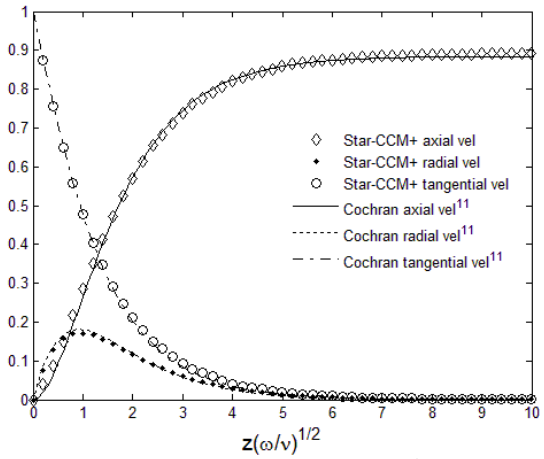

Figure 2. Laminar solution at *Re* = 1000 for the 1x5x5 meter domain, 16x50x50 nodes. *Velocity profiles over the rotating disk:* $u_\theta/\omega r$ (— - — ; o), $u_r/\omega r$ (- - - ; •), $u_z/(\nu\omega)^{1/2}$ (— ; ◊).

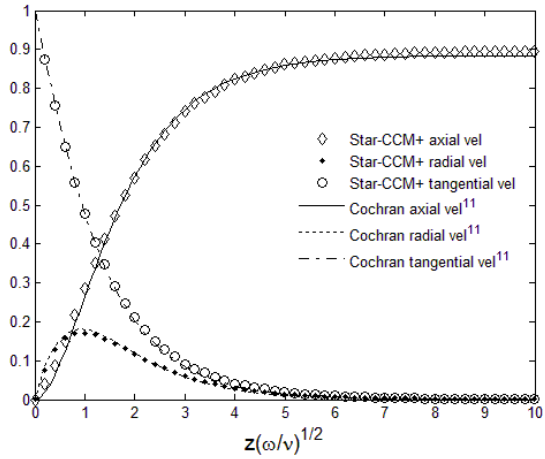

Figure 3. Laminar solution at *Re* = 1000 for the 30x20x20 meter domain, 35x200x200 nodes. *Velocity profiles over the rotating disk. Notations are the same as in Fig. 2*

B. Turbulent Flow

Every turbulence model underwent the same process to find the least computationally expensive grid that did not greatly impact the accuracy of the Star-CCM+[4] solution. The procedure consists of the following steps:

Step 1: The initial cell's centroid was located at y^+ values of 5, 10, 20, 30, 40, 50, 75, 100 and 200. The highest y^+ value at which an acceptable solution was generated, was held constant for all other grid property sensitivity studies.

Step 2: The grid refinements in the radial and tangential directions were varied between the following nodal resolutions: 508x508, 254x254, 127x127, 64x64 and 32x32. The coarsest grid resolution in these two directions that gave a solution comparable with the one obtained with the finest grid, was chosen to be held constant for the future sensitivity studies.

Step 3: The grid's stretch ratio in the axial direction, normal to disk's surface, was varied as: 1.1, 1.2, 1.3, 1.5 and 2.0. The largest stretch ratio that gave a solution comparable with the finest-grid one was set as a constant for future sensitivity simulations.

Step 4: The grid domain size in the radial and tangential directions was varied while the axial dimension remained constant. In this sensitivity study, the computational domain sizes of interest were 1 x 1 meters, 2 x 2 meters, 5 x 5 meters and 10 x 10 meters in the radial and tangential directions. The smallest computational domain size that did not affect the solution was set as a constant for the last step.

Step 5: The computational domain size in the axial direction was altered at this step. The previous simulations used a domain with the velocity inlet located 1 meter above the disk's surface with a prescribed inlet velocity of 1 *m/s*. At this step, the computational domain size was varied to include axial lengths of 0.1, 0.25, 0.5, 1.0, 2.5 and 5.0 meters. This parameter of the grid is not as easily modified as others without having an impact on the flow. The velocity inlet is the only boundary where the flow velocity must be prescribed. The velocity profile varies throughout the domain and prescribing the same velocity at the inlet for all the simulations in this sensitivity study would result in a poor comparison. To remedy this as much as possible, simulations in the largest domain were run with a prescribed inlet velocity of 1 *m/s*. The axial velocity was evaluated at 0.1, 0.25, 0.5, 1.0 and 2.5 meters above the disk's surface and at a radius of 0.421 meters. This radial position was chosen to agree with the sampling point in experiments[14]. These velocities were then used as the prescribed inlet velocities for each simulation respectively. Again, the smallest computational domain size that does not result in a poor solution was sought after.

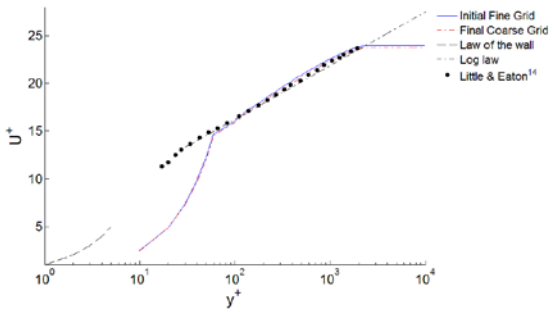

Figure 4. Tangential velocity in rotating reference frame. *Solutions are obtained on the initial fine grid and on the final coarse grid with the standard k-ε turbulence model.*

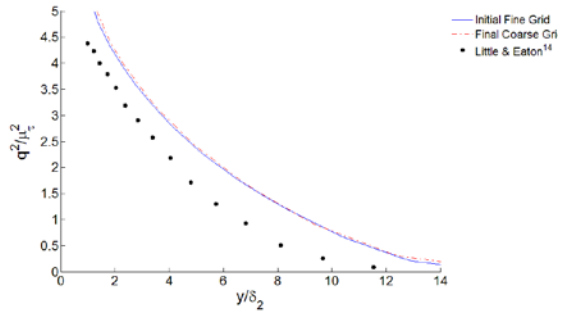

Figure 5. Turbulence kinetic energy. *Solutions are obtained on the initial fine grid and on the final coarse grid with the standard k-ε turbulence model.*

1. Standard *k*-*ε* model

The standard *k*-*ε* turbulence model demonstrated the results stability under most grid parameter changes. The coarse-grid solutions replicated those of the finer grids very closely. Some results are shown in Figs. 4 and 5. All results can be found in Snider[18].

Figure 4 is a semi-logarithmic plot of the tangential velocity in the rotating reference frame plotted in non-dimensional units y^+ vs. U^+. This figure has two analytical solutions imposed onto it along with the experimental data[14]. The near wall curve is the law of the wall, where viscous effects dominate the velocity profile and $U^+ = y^+$. This solution is only valid in the range $y^+ \leq 5$. The log law:

$$U^+ = 2.44 ln y^+ + 5.0$$

is plotted for the range $y^+ \geq 30$. The simulation profiles show close agreement with one another.

Figure 5 shows the profiles of q^2, which is twice the turbulent kinetic energy normalized by the tangential friction velocity μ_τ^2. The horizontal axis is the distance above the disk's surface normalized by the momentum thickness boundary layer, δ_2.

As a weak point, the standard *k*-*ε* turbulence model showed a high sensitivity to highly skewed cells. Cells with the aspect ratios greater than 1000:1 resulted in fatal errors of computations. Here, the aspect ratio of a cell is defined as the relative length of the cell in the tangential (or radial) direction to the length of the cell in the axial direction.

Table 6 compares the grid sizes and computational times of the simulations with the initial (finest) grid selected after Step 1 and with the final (coarse) grid selected after Step 5.

Table 6. Standard *k* - *ε* Computation Comparisons.

	Resolution (nodes)	Cells	Computation Time	Machine
Initial Grid	33 x 508 x 508	8,225,568	5 hours 28 min.	HPC 16 cores
Final Grid	29 x 26 x 26	17,500	3 min. 24 sec.	Desktop 4 cores

To compare with other models, computations with the *k*-*ε* model were also the fastest.

2. Standard *k*-*ω* model

The standard *k*-*ω* turbulence model was robust to most grid parameter changes. Overall, the coarse grids were able to replicate the simulation profiles of finer grids very closely. Some results are shown in Figs. 6 and 7.

Figure 6 is a semi-logarithmic plot of the tangential velocity in the rotating reference frame plotted in non-dimensional units y^+ vs. U^+. The simulation profiles show close agreement with one another.

Figure 7 plots twice the turbulent kinetic energy q^2 normalized by the tangential friction velocity μ_τ^2.

The model, however, showed a high sensitivity to a cells axial stretch ratio (Step 3). Figures 8 and 9 illustrate the problem. Figure 8 is a plot of the radial velocity profiles. There are discrepancies between all simulation profiles. Figure 9 is a plot of the momentum thickness Reynolds number. Again, all simulations have different *Re* values.

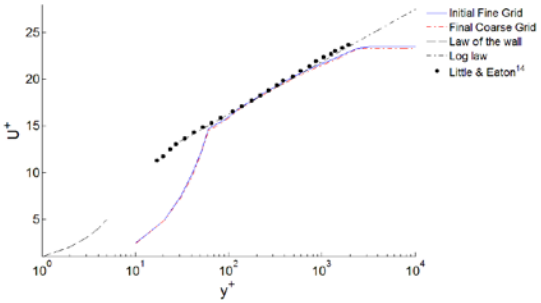

Figure 6. Tangential velocity in rotating reference frame. *Solutions are obtained on the initial fine grid and the final coarse grid with the standard k-ω turbulence model.*

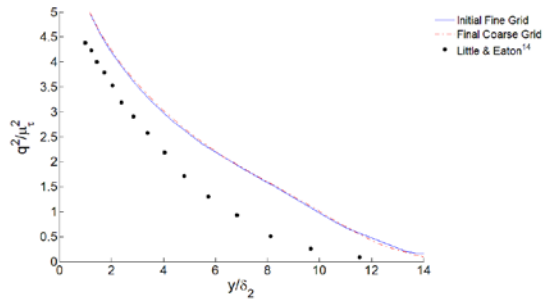

Figure 7. Turbulence kinetic energy. *Solutions are obtained on the initial fine grid and the final coarse grid with the standard k-ω turbulence model.*

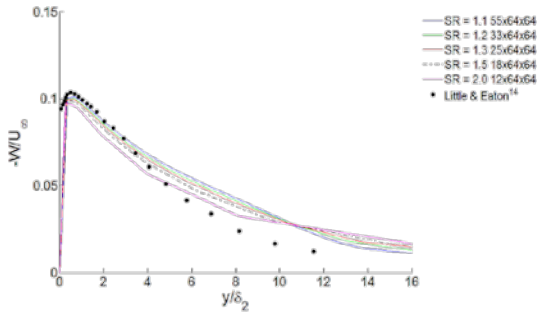

Figure 8. Radial velocity in rotating reference frame. *Comparison of solutions obtained with the standard k-ω turbulence model on grids with varying cell stretch ratios* (SR) *in the axial direction.*

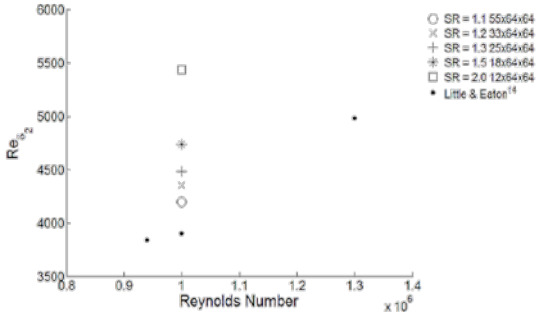

Figure 9. Momentum thickness Reynolds number. *Comparison of solutions obtained with the standard k-ω turbulence model on grids with varying cell stretch ratios* (SR) *in the axial direction.*

Table 7 lists the grid size and computational times of the simulations using the initial (finest) grid selected after Step 1 and using the final (coarse) grid that was selected after Step 5. Computational times of the coarse-grid simulations were much faster compared to those of the fine-grid simulations.

Table 7. Standard *k* - *ω* Computation Comparisons.

	Resolution (nodes)	Cells	Computation Time	Machine
Initial Grid	33 x 508 x 508	8,225,568	5 hours 32 min.	HPC 16 cores
Final Grid	65 x 26 x 26	40,000	4 min. 50 sec.	Desktop 4 cores

3. SST model

The SST turbulence model also demonstrated the ability to tolerate most grid parameter changes. Overall, the coarse grids were able to replicate the simulation profiles of finer grids very closely. Some results are shown in Figs. 10 and 11.

Figure 10 is a semi-logarithmic plot of the tangential velocity in the rotating reference frame plotted in non-dimensional units y^+ vs. U^+. The simulation profiles show close agreement between each other.

Figure 11 plots twice the turbulent kinetic energy q^2 normalized by the tangential friction velocity μ_τ^2.

The SST turbulence model showed a sensitivity to the size of the wall cell. Specifically, the simulation results obtained with the grid where the initial cell's centroid is located at $y^+ = 30$ demonstrated unexpected discrepancies. These discrepancies are possibly due to the initial cell's centroid falling in a "gray area" where the segregation between the *k-ε* and *k-ω* turbulence models has an effect on

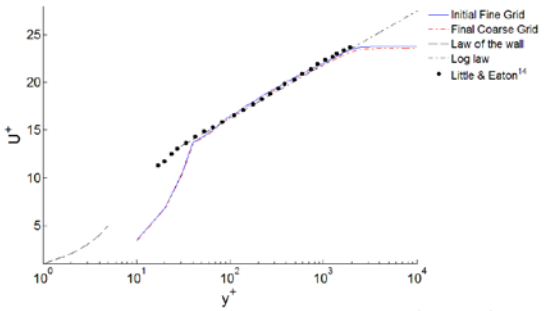

Figure 10. Tangential velocity in rotating reference frame. *Solutions are obtained on the initial fine grid and the final coarse grid with the SST turbulence model.*

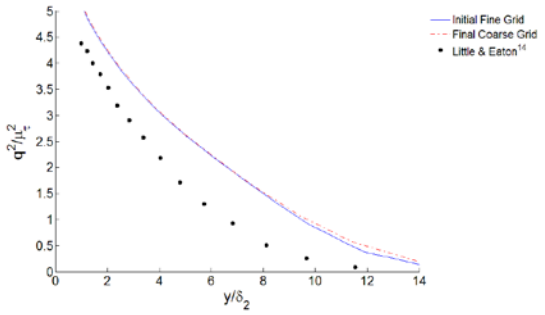

Figure 11. Turbulence kinetic energy. *Solutions are obtained on the initial fine grid and the final coarse grid with the SST turbulence model.*

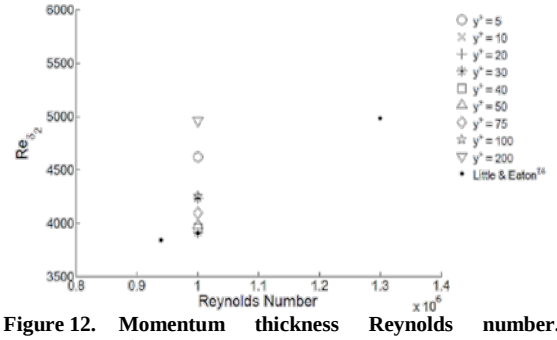

Figure 12. Momentum thickness Reynolds number. *Comparison of solutions obtained with the SST turbulence model on grids with varying y^+ wall cell centroid values.*

the simulation results. One of the examples is given in Fig. 12. The simulation results obtained with y^+ = 10, 20, 40 and 50 have the momentum thickness Reynolds number that agree closely with the experimental data[14], while the Re value obtained with y^+ = 30 deviates from that and is close to the one obtained with y^+ = 100.

Table 8 compares the grid size and computational times of the simulations using the initial (finest) grid selected after Step 1 and using the final (coarse) grid that was selected after Step 5.

Table 8. SST Computation Comparisons.

	Resolution (nodes)	Cells	Computation Time	Machine
Initial Grid	36 x 508 x 508	8,996,715	7 hours 27 min.	HPC 16 cores
Final Grid	41 x 26 x 26	25,000	4 min. 19 sec.	Desktop 4 cores

4. High-Reynolds Number Spalart-Allmaras model

The High-Reynolds Number Spalart-Allmaras turbulence model showed high sensitivity to changes in most grid parameters. Figure 13 shows as an example the radial velocity profile of the simulations with varying initial wall-cell sizes. It is seen that there is disagreement among all simulation profiles.

The axial stretch ratio (Step 3) had the least effect on the solution. However, even in this case, solutions obtained on different grids did not converge to a single profile.

Figures 14 and 15 compare solutions obtained with the finest grid chosen after Step 1 and the coarse grid chosen after Step 5. Figure 14 is a semi-logarithmic plot of the tangential velocity in the rotating reference frame plotted in non-dimensional units y^+ vs. U^+. Figure 15 plots the momentum thickness Reynolds number.

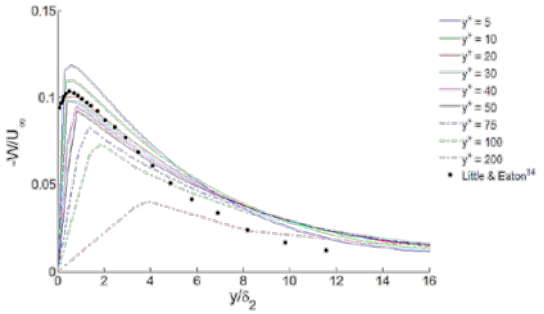

Figure 13. Radial velocity in rotating reference frame. *Comparison of solutions obtained with the High-Re Spalart-Allmaras turbulence model on grids with varying y^+ wall cell centroid values.*

Table 9 compares the grid sizes and computational times of the simulations using initial (finest) grid selected after Step 1 and using the final (coarse) grid that was selected after Step 5.

Table 9. High-Reynolds Number Spalart-Allmaras Computation Comparisons.

	Resolution (nodes)	Cells	Computation Time	Machine
Initial Grid	36 x 508 x 508	8,996,715	5 hours 28 min.	HPC 16 cores
Final Grid	30 x 51 x 51	78,030	6 min. 14 sec.	Desktop 4 cores

Computations with this model required more time due to higher refinement requirements in the radial and tangential direction to compare with other models.

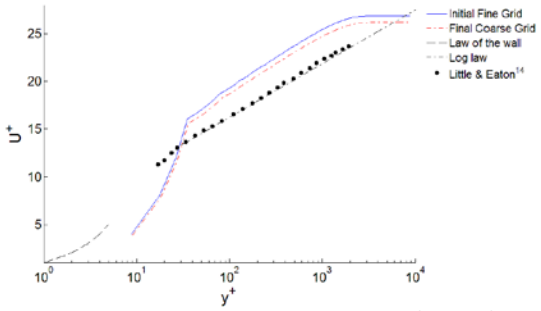

Figure 14. Tangential velocity in rotating reference frame. *Solutions are obtained on the initial fine grid and the final coarse grid with the High-Re Spalart-Allmaras turbulence model.*

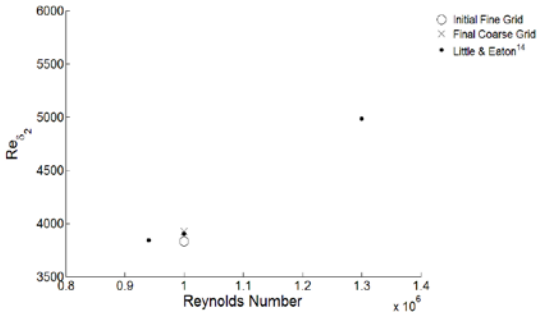

Figure 15. Momentum thickness Reynolds number. *Solutions are obtained on the initial fine grid and the final coarse grid with the High-Re Spalart-Allmaras turbulence model.*

5. Reynolds Stress Transport Model

The RST model was robust to most grid parameter changes. Overall, the coarse grids were able to replicate the simulation profiles of finer grids very closely. Some examples are shown in Figs. 16 and 17.

Figure 16 is a semi-logarithmic plot of the tangential velocity in the rotating reference frame plotted in non-dimensional units y^+ vs. U^+.

Figure 17 plots twice the turbulent kinetic energy q^2 normalized by the tangential friction velocity μ_τ^2.

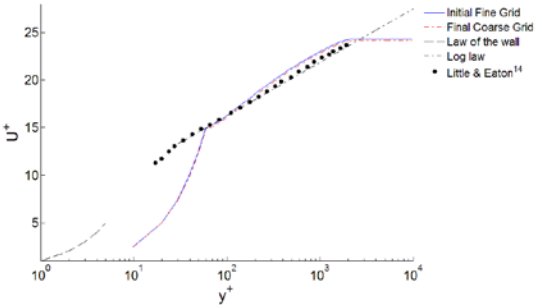

Figure 16. Tangential velocity in rotating reference frame. *Solutions are obtained on the initial fine grid and the final coarse grid with the Reynolds Stress Transport Model.*

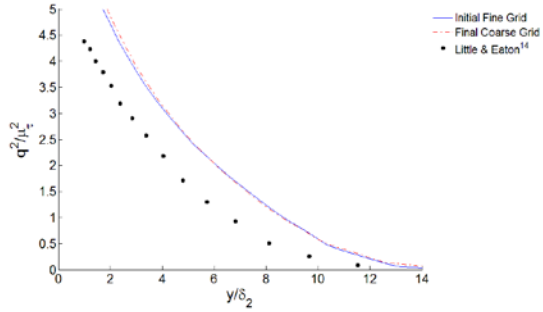

Figure 17. Turbulence kinetic energy. *Solutions are obtained on the initial fine grid and the final coarse grid with the Reynolds Stress Transport Model.*

The RST model showed a sensitivity to the placement of the boundary above the disk's surface (Step 5). This is seen in Fig. 18 as a disagreement between the 5x2x2 meter and the 2.5x2x2 meter domain's simulation profiles. When other turbulence models were used, these two profiles were indistinguishable from one another.

Also, like the standard *k*-ε model, the RST model showed a high sensitivity to highly skewed cells. The presence of cells with the aspect ratio of greater than 1000:1 resulted in fatal errors in Star-CCM+[4].

Table 10 compares the grid sizes and computational times of simulations using the initial (finest) grid selected after Step 1 and using the final (coarse) grid selected after Step 5.

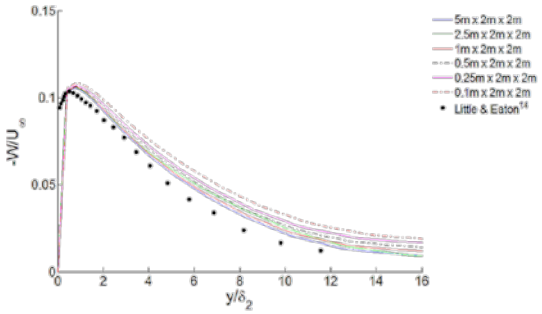

Figure 18. Radial velocity in rotating reference frame. *Solutions are obtained with the Reynolds Stress Transport Model in computational domains with the different placement of the boundary above the disk's surface.*

Table 10. RSTM Computation Comparisons.

	Resolution (nodes)	Cells	Computation Time	Machine
Initial Grid	33 x 508 x 508	8,225,568	9 hours 42 min.	HPC 16 cores
Final Grid	42 x 26 x 26	26,650	6 min. 15 sec.	Desktop 4 cores

In regard of computational time, this is the most demanding model of all models considered in this study.

6. Turbulence Models Comparison

In this section, some of the results for the five turbulence models are compared with one another. (The comparison of all results can be found in Snider[18].) For each turbulence model, results were obtained using a coarse grid found as the most suitable for the model after Step 5 of the sensitivity study procedure.

Figure 19 shows the tangential velocity profiles of each model's simulation. The High-Reynolds Number Spalart-Allmaras turbulence model disagrees with the other model's and the experimental data[14].

Figure 20 shows the radial velocity profiles of each turbulence model's simulation. The *k-ε* and SST simulation profiles slightly overshoot the other models' data near the disks surface.

Table 11 lists the parameters of the coarse grid found through the sensitivity study conducted in Steps 1-5 for each turbulence model. Computational times required to obtain a solution with a given grid are also provided.

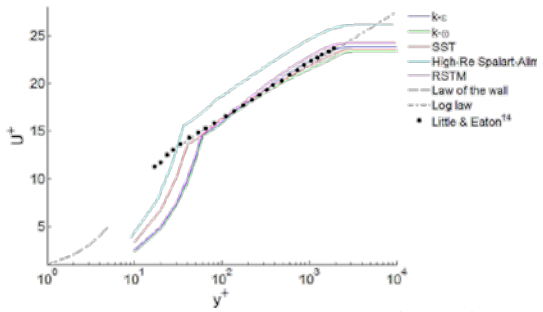

Figure 19. Tangential velocity in rotating reference frame.

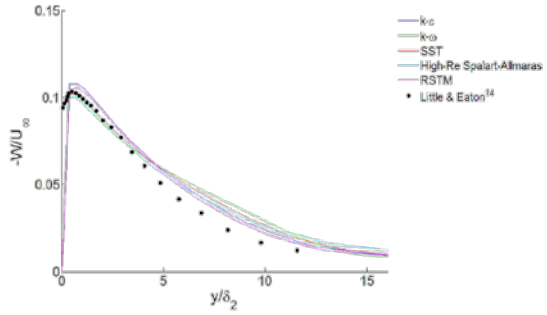

Figure 20. Radial velocity in rotating reference frame.

Table 11. Coarse Grid Properties for all Turbulence Models

	k-ε	*k-* ω	SST	High-Re S-A	RST
y+	30	30	20	20	30
SR	1.3	1.1	1.2	1.3	1.2
Grid (nodes)	29x26x26	65x26x26	41x26x26	30x51x51	42x26x26
Comp. Domain	2.5x2x2 *m*	2.5x2x2 *m*	2.5x2x2 *m*	2.5x2x2 *m*	5.0x2x2 *m*
Comp. Time	03:24 (mm:ss)	04:50 (mm:ss)	04:19 (mm:ss)	06:14 (mm:ss)	06:15 (mm:ss)

VI. Conclusions

As the results show, conducting flow simulations with highly refined grids requires hours on a high performance computer. This option may not be available or affordable for design purposes in industry. Yet, it is essential that computations realistically reproduce the flow features.

To find a reasonable compromise between these requirements, a sensitivity analysis in regard of turbulence models and grid parameters similar to the one described in the current study should be conducted at the initial design stage. The goal of such analysis is to determine i) grid parameters most suitable for the problem and ii) a turbulence model that gives a solution less sensitive to variations in the grid parameters.

In regard to a grid, what was sought in the current study was the coarsest grid that allows one to replicate simulation results obtained with a given turbulence model on more fine grids. It was found that by coarsening a grid in certain ways the time required to complete a simulation can be reduced from hours on high-performance computing facilities to minutes on a local desktop computer without jeopardizing the solution's accuracy.

In regard to a turbulence model, it is important to emphasize that the purpose of this sensitivity study is not to identify a model that produces the most accurate simulation results in comparison with experimental data, but one that is able to replicate results of simulations obtained with finer grids on a coarser grid and is more robust to changes in the gird parameters.

It was found that the High-Reynolds Number Spalart-Allmaras model is the most sensitive to changes in the grid's initial wall-cell length and requires fine grids to obtain results that were still not as accurate as those obtained with other models. In addition, this model, along with the RSTM, required the longest computational time to generate an adequate solution. Due to this reasons, this model although the simplest from all models considered,

cannot be recommended for simulating a flow over a rotating disk and most likely, around and behind a wind turbine.

The standard k-ω model demonstrated the highest sensitivity to changes of the axial stretch ratio. Sensitivity to the other grid parameters was not so pronounced.

The SST model showed a unique sensitivity to the initial wall-cell length. When the near-wall centroid was located at $y^+ = 30$ the simulation results deviated from the results obtained with $y^+ = 20$ and 40. Time required for computations with the SST model was approximately the same as that of for computations with the standard k-ω model.

Simulations with the Reynolds Stress Transport model showed sensitivity to the position of the inlet velocity boundary that was not observed in simulations with other models.

Both the RST and k-ε turbulence models showed high sensitivity to grids containing cells with the high aspect ratio ($\geq$ 1000:1) at the disk's surface. Otherwise, simulations with the k-ε turbulence model were very robust to the grid parameters changes. As a result, this model produced reliable results on the coarsest grid and, thus, in the shortest time.

Utilizing the High y^+ Wall Treatment model allows one to accelerate simulations enormously. The difference in the results obtained using the k-ε model with and without wall treatment (not reported here) was only significant in the region near the disk's surface. (To obtain a solution without wall treatment, a grid should be well refined near a wall.) Thus, if a general picture of the flow structure is of interest rather than the flow physics of the near-wall region, simulations with the High y^+ Wall Treatment model are a far less computationally demanding alternative.

Based on the results of this study, the standard k-ε turbulence model with the High y^+ Wall Treatment is recommended as the turbulence model choice in Star-CCM+[4] for simulations of a flow over a rotating disk.

In the future, this research will be used as a reference for a sensitivity analysis of simulations of a flow around and behind of a wind turbine.

Acknowledgments

The authors express their gratitude to the Center for Advanced Research Computing of the University of New Mexico for providing the access to high-performance computing facilities and consulting support for this research. The authors would also like to thank Prof. Eaton (Stanford University) for helping with the experimental data and CD-adapco for providing Star-CCM+ to the University of New Mexico for academic purposes.

References

[1]IBISWorld. "Wind Power Generation in the US - Industry Market Research Report" IBISWorld.TM-90401, 2011, http://www.evwind.es/noticias.php?id_not=11708.

[2]BTM Consultants. "International Wind Energy Development – World Update 2010."BTM Consultants DK-6950, 2011, http://www.windtoday.net/info/articles_email.html?ID=106940.

[3] Nichols, R. H., and Buning, P. G., "User's Manual for OVERFLOW 2.1," University of Alabama and NASA Langley Research Center, 2008.

[4]Star-CCM+. Computational fluid dynamics solver, Software Package, Ver. 6.02.007, CD-adapco.

[5]Spalart, P. R., and Allmaras, S. R., "A One-Equation Turbulence Model for Aerodynamic Flows," AIAA-92-0439, 1992.

[6]Jones, W. P., and Launder, B. E., "The Calculation of Low-Reynolds Number Phenomena with a Two-Equation Model of Turbulence," *Int. J. of Heat and Mass Transfer*, Vol. 16, 1973, pp. 1119-1130.

[7]Wilcox, D. C., "Reassessment of the Scale-Determining Equation for advanced Turbulence Models," *AIAA Journal*, Vol. 26, No. 11, 1988, pp. 1299-1310.

[8]Menter, F. R., and Rumsey, C. L., "Assessment of Two-Equation Turbulence Models for Transonic Flows," AIAA-94-2343, 1994.

[9] Gibson, M. M., and Launder, B. E., "Ground effects on pressure fluctuations in the atmospheric boundary layer," *J. Fluid Mech.*, Vol. 86, 1978, pp. 491-511.

[10]Von Karman, T., "Uber Laminare und Turbulente Reibung," *Z. Angew. Math Mech*, Vol. 1, 1921, pp. 233-252.

[11]Cochran, W., "The Flow due to a Rotating Disk," *Proceedings of the Cambridge Philosophical Society*, Vol. 30, 1934, pp. 365-375.

[12]White, F., *Viscous Fluid Flow*, 2nd ed., McGraw-Hill, 1991, pp. 154-161.

[13]Xiaohua, W., and Squires, K. D., "Prediction and investigation of the turbulent flow over a rotating disk," *J. Fluid Mech.*, Vol. 418, 2000, pp. 231-264.

[14]Little, H. S., and Eaton, J. K., "Turbulence characteristics of the boundary layer on a rotating disk," *J. Fluid Mech.*, Vol. 266, 1994, pp.175-207.
[15]Kobayashi, R., Kohama, Y., and Takamadate, Ch., "Spiral Vortices in Boundary Layer Transition Regime on a Rotating Disk," *Acta Mechanica*, Vol. 35, 1980, pp. 71-82.
[16]ANSYS ICEM CFD. Fluid and structural meshing program, Software Package, Ver. 13.0, ANSYS.
[17]Lien, F. S., and Leschziner, M. A., "Assessment of turbulence-transport models including non-linear RNG eddy-viscosity formulation and second-moment closure for flow over a backward-facing step," *Computers Fluids*, Vol. 23, 1994, pp. 983-1004.
[18]Snider, M. A., "Sensitivity Study of Turbulent Flow Simulations over a Rotating Disk," M.S. Thesis, Mechanical Engineering Dept., Univ. of New Mexico, Albuquerque, NM, 2012.